Nonadiabatic quantum dynamics in O(3P)+H2→OH+H: A revisited study

ARTICLE *in* JOURNAL OF COMPUTATIONAL CHEMISTRY · DECEMBER 2011

Impact Factor: 3.59 · DOI: 10.1002/jcc.21940 · Source: PubMed

2 AUTHORS:

Boran Han
Harvard University
2 PUBLICATIONS **39** CITATIONS
SEE PROFILE

Yujun Zheng
Shandong University
124 PUBLICATIONS **900** CITATIONS
SEE PROFILE

DOI: 10.1002/jcc.21940

Nonadiabatic Quantum Dynamics in $O(^3P)+H_2 \rightarrow OH+H$: A Revisited Study

Boran Han[a] and Yujun Zheng*[a]

To investigate the extent of nonadiabatic effects in the title reaction, quasi-classical trajectory and nonadiabatic quantum scattering as well as the nonadiabatic quantum-classical trajectory calculations were performed on the accurate *ab initio* benchmark potential energy surfaces of the lowest $^3A'$ and $^3A''$ electronic states [Rogers et al., J Phys Chem A 2000, 104, 2308], together with the spin-orbit coupling matrix [Maiti and Schatz, J Chem Phys 2003, 119, 12360] and the lowest singlet $^1A'$ potential energy surface [Dobby and Knowles, Faraday Discuss 1998, 110, 247]. Comparison of the calculated total cross sections from both adiabatic and nonadiabatic calculations has demonstrated that for adiabatic channels including $^3A' \rightarrow ^3A'$ and $^3A'' \rightarrow ^3A''$, difference does exist between the two kinds of adiabatic and nonadiabatic calculations, showing nonadiabatic effects to some extent. Such nonadiabatic effects tend to become more conspicuous at high collision energies and are found to be more pronounced with trajectories/quantum wave packet initiated on $^3A'$ than on $^3A''$. Furthermore, the present study also showed that nonadiabatic effects can bring the component of forward-scattering in the product angular distributions. © 2011 Wiley Periodicals, Inc. J Comput Chem 32: 3520–3525, 2011

Keywords: nonadiabatic quantum dynamics · potential energy surfaces · cross section · quasiclassical trajectory

Introduction

In the past few years, the reaction $O(^3P)+H_2 \rightarrow OH+H$ has become a pivotal proportion in molecular dynamics, and has therefore received many experimental and time-dependent quantum mechanics (TDQM) as well as quasi-classical trajectory (QCT) studies.[1–28]

The accurate *ab initio* potential energy surfaces for the lowest $^3A'$ and $^3A''$ electronically adiabatic states of reaction O (^3P) $+H_2$ have been calculated by Rogers et al.[1] The resulting fitted PESs are of compelling importance for the studies afterwards.[1–4,20–27] The excitation functions of both TDQM and QCT were presented and compared by Braunstein et al.[2] based on these benchmark potential energy surfaces.[1] In this regard, we should mention the work of Maiti and Schatz[26] and of Chu et al.[3] for initially presenting a semiclassical and an exact quantum study of spin-orbit-induced intersystem crossing effects in the $O(^3P,^1D)+H_2$ reaction. The quantum calculation[3] agrees quantitatively with the QCT surface hopping study.[26] Later, the system was subjected to a nonadiabatic study using trajectory dynamics within the approximate quantum potential approach.[4]

Later, starting from the *ab initio* data of Roger et al.[1] and the double many body expansion formalism, Brandao et al.[29,30] reported a new potential energy surface for the lowest $^3A''$ state by incorporating a semiclassical model of long-range interactions to accurately describe the van der Waals region on the potential energy surface (PES). They found that the well depth of the van der Waals region can have significant impact on the low collision energy behaviors, leading to a three or four times higher cross section at 12.6 kcal/mol when compared with the result from Roger et al.'s surface. This new potential energy surface has also been used in many subsequent studies, such as in location of start tunneling point using a new practical approach,[30] in QCT and quantum mechanical studies with discussions of low-energy dynamical behavoirs,[31,32] chemical stereodynamics studies,[33] etc.

In this work, we mainly focus on examining the extent of nonadiabatic effects in the title reaction over a collision energy range of 0.2–1.2 eV. For this purpose, comparison of the integral cross sections has been made between the adiabatic calculations and the nonadiabatic quantum calculations, between the adiabatic channel and the nonadiabatic channel in the nonadiabatic quantum calculation. Comparison of the angular distributions has also been made between the adiabatic and the nonadiabatic quantum-classical trajectory calculations. In Figure 1, we schematically show the energy profiles along the minimum energy reaction path for the $O(^3P, ^1D)+H_2$ reactive system.[34] Here, the $O(^3P_{2,1,0})+H_2$ reactant correlates to the three triplet states of $^3A''$, $^3A''$ (these first two state are generated ones) and $^3A'$ while $O(^1D)+H_2$ to the singlet state of $^1A'$. As clearly shown, just near the top of the triplet barriers, there are triplet-singlet crossings arising from the spin-orbit couplings. As consequences, part of the wave packet or trajectories that initiated on triplet states will transfer onto the singlet state when the wave packet/trajectory moves near the intersystem crossing region, thus opening nonadiabatic pathways from triplet states to singlet state. Similarly, there also exist the nonadiabatic pathways from one triplet state to another triplet state due to the spin-orbit couplings among the triplet states. These nonadiabatic pathways, as indicated in the figure, also correlate to the OH+H products, indicating that nonadiabatic

[a] *B. Han, Y. Zheng*
School of Physics, Shandong University, Jinan 250100, China
E-mail: yzheng@sdu.edu.cn

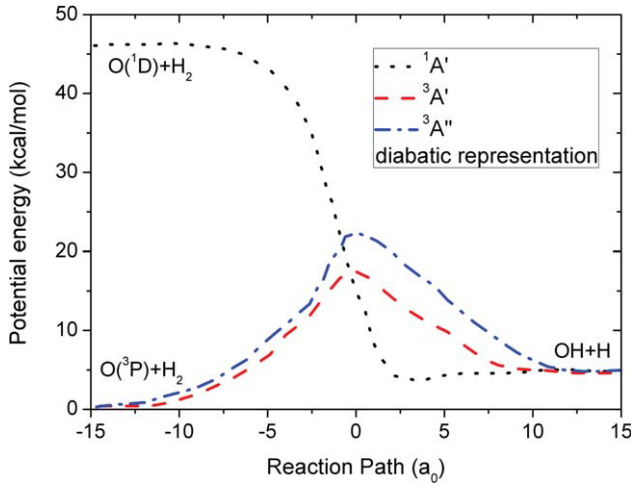

Figure 1. The energy profiles along the minimum reaction path of the $O(^1D,^3P)+H_2$ reactive system taken from Ref. [34]. [Color figure can be viewed in the online issue, which is available at wileyonlinelibrary.com.]

channels can contribute to the formation of the OH+H products. Also from the figure, we can see that the formation mechanisms from the two (adiabatic and nonadiabatic triplet-to-singlet) channels are quite different: the abstract saddle point on the triplet states indicates that in adiabatic channel, it is preferable for O to collinearly collides with H_2 and then abstracts one H from the H_2 molecule to form the products., while in the nonadiabatic triplet-to-singlet channel, an insertion of O into the H_2 molecule to form the products is favorable.

The previous adiabatic quantum and the present adiabatic QCT calculations were performed separately on the $^3A'$ and $^3A''$ electronic states,[2] while the present nonadiabatic quantum and nonadiabatic quantum-classical trajectory calculations were carried out on four-coupled-electronic states (two $^3A''$, $^3A'$ and $^1A'$ with spin-orbit couplings among these states) with the initial wave packet in the $^3A'$ and the two $^3A''$ states, respectively.[3] The adiabatic channels as we denoted here in both adiabatic and nonadiabatic cases are $^3A' \rightarrow ^3A'$ and $^3A'' \rightarrow ^3A''$, while the nonadiabatic channels in the nonadiabatic calculation are $^3A' \rightarrow ^3A''$, $^1A'$ and $^3A'' \rightarrow ^3A'$, $^1A'$. We noted here that in nonadiabatic case, results for the adiabatic channels $^3A' \rightarrow ^3A'$, $^3A'' \rightarrow ^3A''$ still receive contributions from nonadiabatic effect, due to these results are generated from a multisurface calculation.

This article proceeds as follows: the calculation methods are concisely described in Computational Aspects Section. We present the calculated results and the comparison among the adiabatic and nonadiabatic studies with discussion of the nonadiabatic effects in Results and Discussion Section. Conclusion is given at the last section.

Computational Aspects

All the adiabatic calculations used the benchmark PESs of $^3A'$ and $^3A''$ fitted by Rogers et al.[1]. During the fitting procedure, two different fitting methods have been chosen, the rotating morse spline (ROMS) and the generalized London-Eyring-Polanyi-Sato double-polynomial methods. Both methods have been shown to satisfy most of the criteria with several successful applications. Detailed features of these two triplet potential energy surfaces can be found in Ref. [1]. In the nonadiabatic calculations, these triplet surfaces are used together with the PES of the singlet $^1A'$ state of Dobbyn and Knowles (DK)[35] (that is, the PESs for triplet and singlet states constitute the diagonal elements of the diabatic potential matrix) and with the spin-orbit coupling matrix of Maiti and Schatz[26] (it constitutes the off-diagonal part of the diabatic potential matrix), and interested readers can refer that work for details of this matrix.

The adiabatic QCT calculation method we adopted in this study is the same as the ones described in refs. 28, 36–39. That is, standard Monte Carlo techniques[37] were used, and the classical Hamilton's equations were integrated for motion in three dimensions. A batch of 50,000 trajectories were running on each electronic state after setting the initial rovibrational state of the H_2 reactant to be $v = 0$ and $j = 0$. For each of collision energy in the range of 0.2–1.2 eV, optimization of the maximum impact parameter was carried out first and the appropriate one was thus determined for the subsequent calculation. A fixed time step of 0.1 fs was found enough for the conservation of the total energy and total angular momentum.

The nonadiabatic quantum calculations for $O(^3P)+H_2$ were done using the nonadiabatic time-dependent wave packet approach,[3,40–42] This approach includes three steps, (i) construction of initial wave packet in a column vector form, (ii) propagation of the initial wave packet with an extended split-operator scheme developed to treat the multi-state scattering problems, and (iii) analysis of the final wave packet to extract the total reaction probabilities and thus the total reaction cross sections.

Specifically, the corresponding Schrödinger equation to be solved is formulated in terms of the diabatic electronic basis,[40,41]

$$i\frac{\partial}{\partial t}\begin{bmatrix}\phi_{3A''(1)}\\ \phi_{3A''(2)}\\ \phi_{3A'}\\ \phi_{1A'}\end{bmatrix} = \left(\hat{T}\begin{bmatrix}1&0&0&0\\0&1&0&0\\0&0&1&0\\0&0&0&1\end{bmatrix}\right.$$

$$+\begin{bmatrix}PES_{3A''(1)}&0&0&0\\0&PES_{3A''(2)}&0&0\\0&0&PES_{3A'}&0\\0&0&0&PES_{1A'}\end{bmatrix}$$

$$\left.+\begin{bmatrix}0&0&SO_{3A''(1)-3A'}&SO_{3A''(1)-1A'}\\0&0&SO_{3A''(2)-3A'}&SO_{3A''(2)-1A'}\\SO_{3A''(1)-3A'}&SO_{3A''(2)-3A'}&0&SO_{3A'-1A'}\\SO_{3A''(1)-1A'}&SO_{3A'(2)-1A'}&SO_{3A'-1A'}&0\end{bmatrix}\right)\begin{bmatrix}\phi_{3A''(1)}\\ \phi_{3A''(2)}\\ \phi_{3A'}\\ \phi_{1A'}\end{bmatrix}$$

$$T = \frac{1}{2\mu_R}\frac{\partial^2}{\partial R^2} + \frac{1}{2\mu_r}\frac{\partial^2}{\partial r^2} + \frac{(\hat{J}-\hat{j})^2}{2\mu_R R^2} + V(r)$$

And the present nonadiabatic results were generated with the initial populated state of the wave packet being the $^3A'$ and the two $^3A''$ ones, respectively. That is to say, we carried out three nonadiabatic quantum scattering

calculations, with the initial wave column vector to be set as $\begin{bmatrix}\phi_{^3A''(1)}\\0\\0\\0\end{bmatrix}$ and $\begin{bmatrix}0\\\phi_{^3A''(2)}\\0\\0\end{bmatrix}$ and $\begin{bmatrix}0\\0\\\phi_{^3A'}\\0\end{bmatrix}$ separately.

The extended split-operate scheme that is used to propagate the initial wave packet (in other words, to numerically solve the equation) and the construction method of the initial wave packet as well as the meaning of the symbols of R, r, ***J***, ***j*** and V(r), etc, in the above equations, and how to carry out the final analysis can be referred from Refs. [40] and [41]. We note here that our analysis of the propagated wave packet has been implemented in a way to distinctly discriminate the adiabatic channel and nonadiabatic channels. For example, in the calculation with initiate $^3A''(1)$ state, we performed analysis for the adiabatic channel using the wave packet component of $\Phi_{^3A''(1)}$, while the results for nonadiabatic channel are obtained by summing over the analyzed result using the other three components of $\Phi_{^3A''(2)}$, $\Phi_{^3A'}$ and $\Phi_{^1A'}$.

The nonadiabatic quantum results we obtained here just reproduced from the previous benchmark work of Chu et al.[3,40] The convergence parameters used in the quantum calculations are the same as those in Ref. [3]: the propagation time was 25,000 a.u., the number of translational and vibrational basis functions was 200 and 100, and a $j_{max} = 68$ for rotational basis functions. The *R* and *r* coordinate ranges were 0.0–15.0 and 0.5–11.5 a_0, respectively.

Moreover, we also carried out the nonadiabatic quantum-classical trajectory calculations to obtain the information on product angular distributions for the title reactive system. This nonadiabatic method is based on the coherent switching with decay of mixing (CSDM) theory of Truhlar and coworkers,[43,44] and the corresponding computational code we used here is developed by Han and coworkers.[45,46] Briefly speaking, in the CSDM theory for a multistate system, the nuclear motion is still governed by the semiclassical Hamilton's motion equation. And all the relevant physical quantities associated with the electronic motion, such as the electronic density matrix elements, essentially have two parts: the fully coherent part and the decay of mixing part. Most of the quantum effects are included in the coherent part, while the decay of mixing part leads to decoherence of the time-evolved electronic matrix, which is determined by the switching probability. The probability of switching the decoherent state is formulated in terms of the electronic Hamiltonian matrix elements, the electronic density matrix elements. And the evolution of the electronic state populations is governed by the time-dependent electronic Schrödinger equation in terms of electronic density matrix elements. The switching scheme in CSDM can treat each complete passage of a strong coupling region coherently by giving modifications to a coherent set of state populations (the virtual state populations) based on the judgment of the intensity of nonadiabatic coupling along the trajectory.[43] In this quantum-classical trajectory calculation, we used the same potential matrix (i.e., the electronic Hamiltonian matrix) as that in the nonadiabatic quantum scattering calculation, and the integration step in solution of the Hamilton's equation is set to be 0.05 fs. Information on product angular distributions can be obtained by carrying out the corresponding analysis for each of the involved four electronic states according to the final information of the nuclear trajectories. More details about this computational method and computational code as well as the computational aspect can be found in Refs. [43–46].

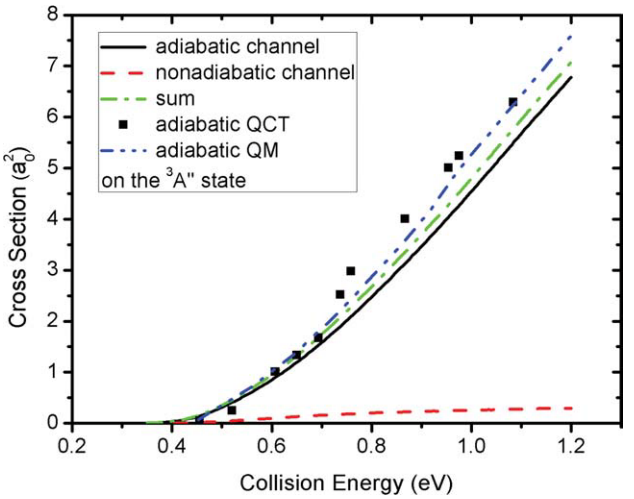

Figure 2. Total reaction cross sections as a function of collision energy in the range of 0.1–1.2 eV. Here the wave packet/trajectory is initiated on $^3A''$. Adiabatic QM results taken from Ref. [2].

Results and Discussion

Figure 2 shows the total reaction cross sections as a function of collision energy, generated from the adiabatic QCT calculations running on the $^3A''$ electronic state, together with the results of both adiabatic and nonadiabatic channels as well as the summed values over both channels from the nonadiabatic quantum scattering calculations with the initial wave packet starting in the same electronic state. Also shown are the corresponding results from a previously adiabatic quantum scattering calculation[2] on $^3A''$. As mentioned above, two $^3A''$ are involved in the nonadiabatic calculation that requires propagating wave packet twice with initial wave packet starting individually in each of the two $^3A''$ states. To compare with the adiabatic QCT and quantum calculated results, in this figure, we just averaged the calculated results from the nonadiabatic quantum scattering calculations according to $[^3A''\ (1)+{}^3A''\ (2)]/2$. Figure 3 are the corresponding results associated with the $^3A'$ electronic state. As seen, all the calculated results show a threshold at low collision energy and increase with the increasing of the collision energy. This substantiates the properties of the $^3A''$ and $^3A'$ PESs, which have a barrier height of 14.1 kcal/mol ($\sim$ 0.61eV).[1] The $^3A'$ surface has a deeper bending curve than the $^3A''$ surface leading to significantly different reaction cross sections on the two surfaces.[19] From the figures, we can see clearly that the results of the QCT and TDQM adiabatic methods match well with each other, except at collision energy near threshold and at high collision energy in the $^3A'$ case.

Comparison of the summed values over the two kinds of adiabatic and nonadiabatic channels with the results of the

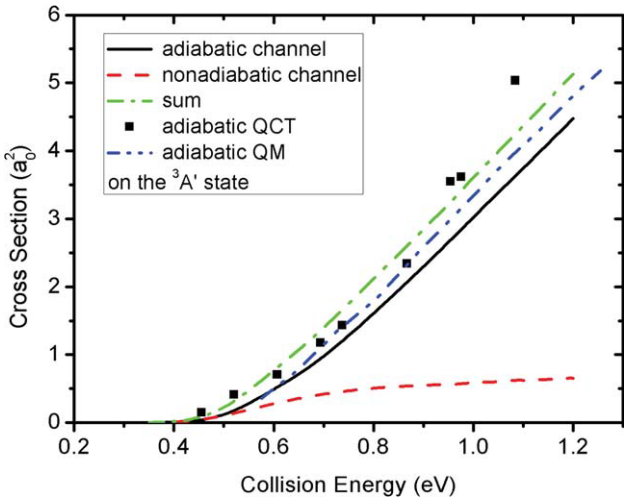

Figure 3. Same as Figure 1, but on $^3A'$.

adiabatic channel, generated from the nonadiabatic quantum scattering calculations, provides here an unequivocal evidence for the influence of nonadiabatic effects on the underlying reaction mechanism. It is found that nonadiabatic effects become gradually strong with increasing collision energies for both triplet electronic states. In addition, comparison of the nonadiabatic calculation results between the two figures revealed that nonadiabatic effects are much more pronounced in the $^3A'$ case than in the $^3A''$ case.

Now let us turn to comparison between the two quantum scattering calculations, i.e., the previous adiabatic and the present nonadiabatic ones. This comparison shows that the summed values from the nonadiabatic calculation are smaller than those from the adiabatic calculation in the $^3A''$ case while they are larger than the corresponding adiabatic values in the $^3A'$ case. Such observed differences can be explained with the spin-orbit splitting. As shown in Figure 4, consideration of the spin-orbit couplings in the nonadiabatic calculation, leads to the energy splitting correlates with the reactant fine structure $O(^3P_2,^3P_1,^3P_0)+H_2$, thus resulting in the lowered and increased barrier height on the the $^3A'$ and $^3A''$ PESs used in the nonadiabatic calculation. Therefore this can account for the differences between the two kinds of quantum calculations.

Fortunately, such influence due to the inclusion of spin-orbit couplings in nonadiabatic calculation is completely washed out when statistically calculating the averaged total reaction cross sections by (1/3)(Figs. 1 and 2), as revealed in Figure 5 where such statistically averaged total reaction cross sections are plotted as a function of collision energy, in conjunction with the statistical averaged results of Braunstein et al.[2] deduced by $(1/3)(^3A''+^3A')$ from their calculated cross sections on the separate $^3A''$ and $^3A'$ surfaces without couplings between them. In this figure, we can see that the statistical summed results over the adiabatic and nonadiabatic channels are identical to those purely adiabatic quantum results, satisfying the conservation law of total reaction cross section. Interestingly, Garashchuk et al.[4] have previously reported similar conservation of the calculated reaction probabilities for $J = 0$ in their nonadiabatic dynamics explorations on the $O(^3P, ^1D)+H_2$ system. A nonadiabatic study by Chu et al.[47] has also reported such conservation of the total reaction cross sections in the DH_2^+ and HD_2^+ systems. Hence, the conversation of the integral cross sections has further confirmed the correctness of our present nonadiabatic quantum calculations. In addition, we can see there is a qualitative agreement between the QCT and the quantum calculations in Figure 5, and it is much better than the agreement illustrated in Figures 2 and 3 with the initial wave packet on the two separate triplet states. The corresponding experimental measurements of the excited functions[48] are also included in Figure 5 to make a comparison, showing a very good agreement between theory and experiment.

Again, for the adiabatic channel, comparison of the total cross sections between the adiabatic and nonadiabatic calculations demonstrated difference that tends to increase with increasing collision energy, thus also indicated a gradually stronger influence of the nonadiabatic effects at higher collision energy. This is in consistent with the previous observations as seen from Figures 2 and 3.

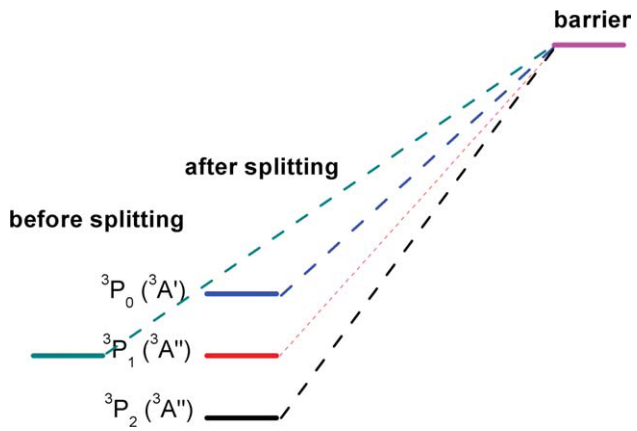

Figure 4. Sketch map for energy profile of the reaction system before and after the spin-orbit splitting.

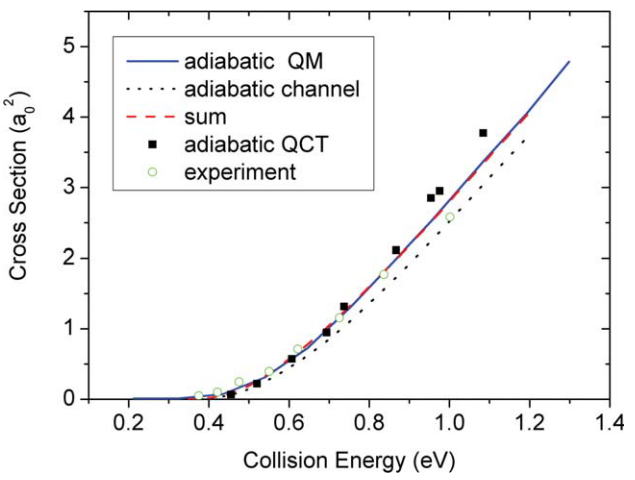

Figure 5. Statistically averaged total cross sections as a function of collision energy ranging from 0.2 to 1.2 eV. Adiabatic QM results taken from Ref. [2], and experimental measurements taken from Ref. [48].

Overall, this revisited study of the $O(^3P)+H_2$ reaction has presented some evidence for the influential nonadiabatic effects on the underlying mechanism. Nonadiabatic effects are found to be responsible for the observed differences between the calculated integral cross sections from the adiabatic and nonadiabatic calculations. But such difference is perhaps not significantly large and therefore can not show any sign in the measured excitation functions. This can explain why there are no experimental reports with respect to this thus far.[49] However, very recently, in a combined experimental and theoretical study of the $O(^3P)+D_2$ reaction, Garton et al.[50] suggested a measurable but minor nonadiabatic effect for this reaction system, from the presence of the lower translational energy distributions and some forward scattering in the angular distribution for the product OD in the comparison between theory and experiment.

For further revealing the nonadiabatic effects in the context of state-to-state dynamics, in Figure 6, we present our calculated differential cross sections at the collision energy of 1.2 eV from the trajectory calculations for the trajectories initiated on the $^3A''$ and $^3A'$ states, respectively. For the adiabatic channel of $^3A''\rightarrow{}^3A''$ or $^3A'\rightarrow{}^3A'$, the corresponding results from the adiabatic QCT and the nonadiabatic quantum-classical trajectory calculations are both presented, and it can be seen that the two kinds of trajectory calculations predicted quite similar shape for the angular distributions. For the nonadiabatic channels, we adopted the same strategy to treat and analyze the corresponding results as we have stated before. As can be seen, these angular distributions showed some differences between the adiabatic and the nonadiabatic channels concerning both triplet states. The products formed through the nonadiabatic channels exhibit a broad angular distribution with the presence of some forward-scattering, while the backward-scattering is relatively dominant in the angular distributions of those formed through the adiabatic channels. Thus, our present calculations have also showed that nonadiabatic effects can have some impact on the state-to-state reaction dynamics of the $O(^3P)+H_2$ reaction by bring some forward-scattering components in the angular distributions. And this phenomenon agrees well with that revealed for its heavy isotope variant in the previous experimental and theoretical combined study.[50] The presence of forward-scattering is due to the involvement of the singlet state in the multiple-state reaction mechanism, and thus the influence and the interference of the insertion mechanism, since it is known that product angular distribution should have forward-backward symmetry for a typical insertion mechanism. Therefore, although nonadiabatic effects are not obviously showing up in the measured excitation functions in $O(^3P)+H_2$, there may have a possibility for them to be experimentally fingerprinted in the measured product angular distribution, just like its heavy isotope variant.[50]

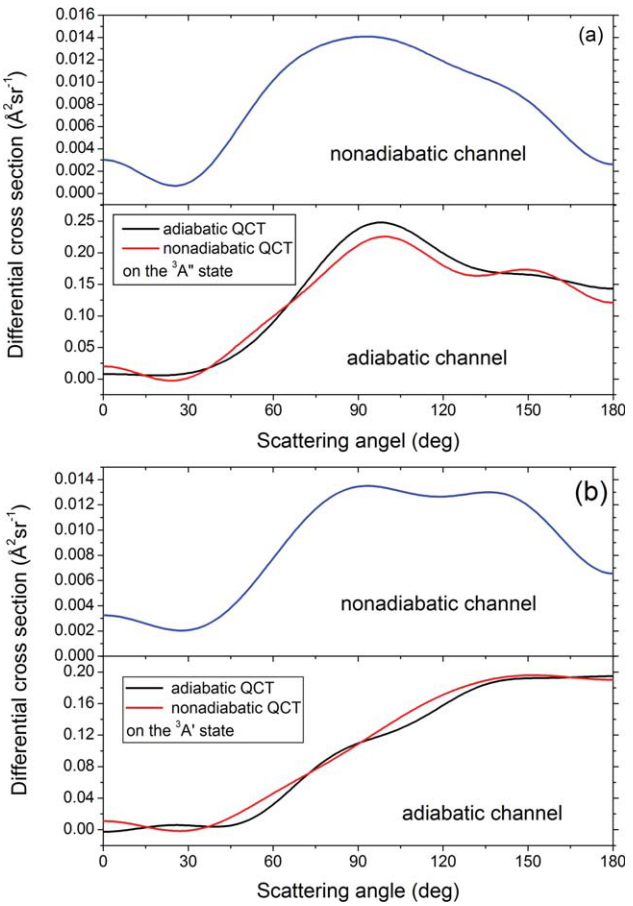

Figure 6. The calculated product angular distributions of the adiabatic and nonadiabatic channels for trajectories initiated on (a) the $^3A''$ electronic state and (b) the $^3A'$ electronic state. [Color figure can be viewed in the online issue, which is available at wileyonlinelibrary.com.]

Conclusions

By carrying out the adiabatic QCT and the nonadiabatic quantum scattering as well as the nonadiabatic quantum-classical trajectory calculations and with combination of the previous adiabatic quantum calculations, we presented here a study of the nonadiabatic effects in the title reaction system. In all calculations, the benchmark $^3A'$ and $^3A''$ potential energy surfaces of Roger et al.[1] are used. In addition, nonadiabatic quantum scattering calculations and nonadiabatic quantum-classical trajectory calculations also used the spin-orbit coupling matrix of Maiti and Schatz[26] and the DK potential energy surface of the singlet $^1A'$ state.[34]

Comparison of the calculated total cross sections between/among the adiabatic and nonadiabatic calculation methods, demonstrated, to some extent, the existence of the nonadiabatic effects in the underlying reaction mechanism. Influence of nonadiabatic effects is found to become gradually pronounced with an increase of the collision energy. Further, when the trajectory/wave packet is initiated on the $^3A'$ state, there are much more nonadiabatic effects in the underlying reaction mechanism. The statistical total cross sections satisfy the conservation law, which supports the validity of present calculations. Finally, comparison of the calculated product angular distributions between the adiabatic channel and the nonadiabatic channel has also showed the influences of

nonadiabatic effects on state-to-state reaction dynamics, with the presence of some forward-scattering in the angular distributions for products formed through the nonadiabatic channels. This is in consist with the previous study of the $O(^3P)+D_2$ reaction.[50] The present theoretical study thus predicted a possibility for fingerprinting the nonadiabatic effects of the title reactive system in the measured differential cross sections.

[1] S. Rogers, D. Wang, A. Kuppermann, J Phys Chem A 2000, 104, 2308.
[2] M. Braunstein, S. Adler-Golden, B. Maiti, G. C. Schatz, J Chem Phys 2004, 120, 4316.
[3] T. S. Chu, X. Zhang, K. L. Han, J Chem Phys 2005, 122, 214301.
[4] S. Garashchuk, V. A. Rassolov, G. C. Schatz, J Chem Phys 2006, 240, 244307.
[5] M. Broida, A. Persky, J Chem Phys 1984, 80, 3687.
[6] D. W. Schwenke, J Chem Phys 1993, 98, 342.
[7] R. E. Howard, A. D. McLean, W. A. Lester,Jr., J Chem Phys 1979, 71, 2412.
[8] M. J. T. Jordon, K. C. Thompson, M. A. Collins, J Chem Phys 1994, 102, 5647.
[9] T. Joseph, D. G. Truhlar, B. C. Garrett, J Chem Phys 1988, 88, 6982.
[10] K. T. Lee, J. M. Bowman, A. F. Wagner, G. C. Schatz, J Chem Phys 1982, 76, 3563.
[11] K. T. Lee, J. M. Bowman, A. F. Wagner, G. C. Schatz, J Chem Phys 1982, 76, 3583.
[12] G. C. Light, J Chem Phys 1978, 68, 2831.
[13] K. A. Peterson, T. H. Dunning,Jr., J Phys Chem A 1997, 101, 6280.
[14] N. Presser, R. J. Gordon, J Chem Phys 1985, 82, 1291.
[15] G. C. Schatz, J Chem Phys 1985, 83, 5677.
[16] G. C. Schatz, A. F. Wagner, S. P. Walch, J. M. Bowman, J Chem Phys 1981, 74, 4984.
[17] R. Schinke, W. A. Leater,Jr., J Chem Phys 1979, 70, 4893.
[18] S. P. Walch, J Chem Phys 1987, 86, 5670.
[19] S. P. Walch, T. H. Dunning,Jr.;R. C. Raffenetti, F. W. Bobrowicz, J Chem Phys 1980, 72, 406.
[20] S. Atahan, J. Klos, P. S. Zuchowski, M. H. Alexander, Phys Chem Chem Phys 2006, 8, 4420.
[21] S. Garashchuk, V. A. Rassolov, G. C. Schatz, J Chem Phys 2006, 124, 244307.
[22] P. F. Weck, B. J. Balakrishnan, C. Rosa, W. Wang, J Chem Phys, 2006, 124, 074308.
[23] W. Wang, C. Rosa, J. Brandao, Chem Phys Lett 2006, 418, 250.
[24] P. F. Weck, N. Balakrishnan, J Chem Phys 2005, 123, 144308.
[25] N. Balakrishnan, J Chem Phys 2004, 121, 6346.
[26] B. Maiti, G. C. Schatz, J Chem Phys 2003, 119, 12360.
[27] N. Balakrishnan, J Chem Phys 2003, 119, 195.
[28] X. Zhang, K. L. Han, J Chem Phys 2003, 106, 1815.
[29] J. Brandao, C. Mogo, B. C. Silva, J Chem Phys 2004, 121, 8861.
[30] C. Rosa, J. Brandao, Chem Phys Lett 2008, 461, 150.
[31] W. L. Wang, C. Rosa;J. Brandao, Chem Phys Lett 2006, 418, 250.
[32] P. F. Weck, N. Balakrishnan, J. Brandao, C. Rosa, W. Wang, J Chem Phys 2006, 124, 074308.
[33] Q. Wei, X. Li, T. Li Chem Phys 2010, 368, 58.
[34] B. Maiti, G. C. Schatz, J Chem Phys 2003, 119, 12360.
[35] J. Dobbyn, P. J. Knowles, Faraday Discuss 1998, 110, 247.
[36] K. L. Han, G. C. He, N. Q. Lou J Chem Phys 1996, 105, 8699.
[37] D. G. Truhlar, J. T. Muckerman, In Atom-Molecules Collision Theory; R. B. Bernstein, Ed.; Plenum Press; New York, 1979.
[38] L. M. Raff, D. L. Thompson, In Thoery of Chemical Reaction Dynamics; M. Baer Ed.; CRC Press: Boca Raton, 1985.
[39] J. N. Murrell, S. Cancer, S. C. Farantos, P. Huxley, A. J. C. Varandas, Molecules Collision Theory; Plenum Press: New York, 1979.
[40] T. S. Chu, Y. Zhang, K. L. Han, Int Rev Phys Chem 2006, 25, 201.
[41] T. X. Xie, Y. Zhang, M. Y. Zhao, K. L. Han, Phys Chem Chem Phys 2003, 5, 2034.
[42] (a) T. S. Chu, K. L. Han, Phys Chem Chem Phys 2008, 10, 2431; (b) T. S. Chu, K. L. Han, J Phys Chem A 2005, 109, 2050; (c) J. Hu, K. L. Han, G. Z. He, Phys Rev Lett 2005, 95, 123001;T. S. Chu, K. L. Han, G. C. Schatz, J Phys Chem A 2007, 111, 8286.
[43] C. Zhu, S. Nangia, A. W. Jasper, D. G. Truhlar, J Chem Phys 2004, 121, 7658.
[44] S. C. Cheng, C. Zhu, K. K. Liang, S. H. Lin, D. G. Truhlar, J Chem Phys 2008, 129, 024112.
[45] B. Li, T. S. Chu, K. L. Han, J Comput Chem 2010, 31, 362.
[46] B. Li, K. L. Han, J Phys Chem A 2009, 113, 10189.
[47] T. S. Chu, A. J. C. Varandas, K. L. Han, Chem Phys Lett 2009, 471, 222.
[48] D. J. Garton, T. K. Minton, B. Maiti, D. Troya, G. C. Schatz J Chem Phys 2003, 118, 1585.
[49] N. Balakrishnan, J Chem Phys 2004, 121, 6346.
[50] D. J. Garton, A. L. Brunsvold, T. K. Minton, D. Troya, B. Maiti, G. C. Schatz, J Phys Chem A 2006, 110, 1327.

Received: 5 April 2011
Revised: 31 July 2011
Accepted: 15 August 2011
Published online on 21 September 2011